Performance analysis of a hydraulic tidal turbine for seawater desalination

A. Jarquin Laguna and F. Greco

Abstract—**Tidal energy is increasingly recognized as a viable renewable energy source with applications extending beyond electricity generation, including seawater desalination for coastal and off-grid communities. This study investigates a novel direct-driven tidal desalination system that eliminates intermediate electrical conversion by mechanically coupling a horizontal-axis tidal turbine to a high-pressure positive displacement pump and a Seawater Reverse Osmosis system with an integrated energy recovery device. The system converts the mechanical power of the turbine into hydraulic energy, driving pressurized seawater through reverse osmosis membranes to produce freshwater, while the brine is recirculated through the Energy Recovery Device to improve efficiency. A time-domain numerical model simulates the system's performance in the below-rated, variable-speed operational range for two configurations under steady-state and turbulent tidal flow conditions. Results indicate that the proposed variable displacement configuration maintains a constant tip speed ratio and offers more stable operation. A 140 kW rotor is capable of producing up to 88.3 m3/h of freshwater at rated current speed, with a specific energy consumption of 3.2 kWh/m3. Under turbulent flow conditions, it achieved an 8% increase in freshwater production and lower pressure fluctuations while maintaining a constant recovery rate. These findings suggest that active hydraulic control enhances the efficiency, stability, and freshwater output of direct-driven tidal desalination systems. However, practical constraints such as membrane flow limits, cavitation risk, and rotor fatigue at high speeds must be addressed in future design considerations.**

Index Terms—**Tidal energy, Seawater desalination, Reverse Osmosis, Numerical modeling**

I. Introduction

TIDAL energy has emerged as a promising source of renewable energy in recent years and its potential applications extend beyond electricity generation. Seawater desalination is a critical process in many water-scarce regions around the world, and renewable energies can be harnessed to power this process [1], [2].

The combination of tidal energy and seawater desalination has several advantages, including a low carbon footprint, high reliability and stable energy output [3]. The technical and economic challenges for such integration are not unique to tidal energy technologies. In particular the performance of a Seawater Reverse Osmosis (SWRO) membrane under variable pressure and flow conditions is a relevant topic to all forms of intermittent renewable energy [4]. Recent work includes the experimental performance evaluation of SWRO for a marine current device [5], as well as for wave energy applications [6], [7] including the use of energy recovery device (ERD) [8]. Regarding wind energy applications, several advances have been made in the integration of desalination systems with horizontal axis turbines as presented in [9], [10]. One of the practical advantages of using hydrokinetic turbines, is the lower power ratings compared with wind turbines which allow to use off-the shelf hydraulic components. At the same time, the high pressure pumps are already located under water so there is no need for priming the seawater flow. Tidal energy for seawater desalination is a promising area of research that could help meet the growing demand for clean drinking water in coastal regions and for off-grid applications.

In previous studies, it is proposed to use a high pressure pump coupled to the rotor with a fixed volumetric displacement, where the control of the rotor speed is achieved indirectly by adjusting the system pressure through the boost pump and the energy recovery device (ERD) [11], [12]. The results of the work presented in [12] showed that this control strategy is in principle feasible for a hydrokinetic device operating below the rated current speed. A wide operating range of the ERD system is required, resulting in recovery rates up to 80% when the operation is close to the rated current speed conditions. However, in practice, the pressure is limited by the operating range and maximum recovery rate of the ERD system, with typical values up to 50% [13]. Thus, limiting the recovery rate to a maximum value leads to a decrease in maximum torque, and resulting in a higher range of operating rotor speeds as well as tip speed ratios as shown in [14].

To overcome these constraints, this work explores an alternative configuration in which the integrated rotor pump has the capability of adjusting the amount of seawater flow rate by modifying its volumetric displacement, i.e. the pump can be actively controlled. Despite the increased complexity, the extra degree of freedom is expected to allow the device to operate at optimal hydrodynamic performance in the below rated variable speed region.

This study contributes to the literature by presenting a performance comparison between the two configurations and control strategies for a direct-driven tidal desalination system with an energy recovery device. The primary objective is to analyse the behaviour of the turbine based on the operational rotor speeds and system pressures for each configuration. The secondary

A. Jarquin Laguna is with the Department of of Maritime & Transport Technology, Faculty of Mechanical Engineering, Delft University of Technology, The Netherlands (e-mail: A.JarquinLaguna@tudelft.nl).

Digital Object Identifier:
https://doi.org/10.36688/ewtec-2025-919

objective is to compare the performance of the SWRO system in terms of freshwater production and specific energy consumption (SEC). Numerical simulations of a single tidal unit are carried out under steady-state and under turbulent tidal flow conditions for a single operating case.

A. Direct-driven hydraulic tidal turbine with energy recovery device

The desalination process without intermediate electrical conversion from tidal energy is proposed as direct-driven desalination. This is possible with the direct integration of a turbine rotor with a hydraulic transmission and a SWRO system. A schematic of the proposed configuration is shown in Fig. 1.

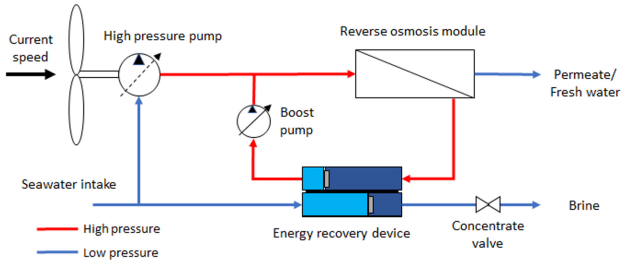

Fig. 1. Schematic of the direct driven tidal stream SWRO system with energy recovery device. The high pressure and the boost pump have active controlled capability indicated by the diagonal arrow.

The proposed configuration consists of a positive displacement high pressure-pump which converts the mechanical power of a horizontal axis rotor into hydraulic power in the form of a pressurized seawater flow. The seawater flow rate is directed to reverse osmosis membranes, where a permeate flow of fresh water is obtained from the pressure difference between the high-pressure feed and the membranes' osmotic pressure. The remaining brine is circulated through an ERD and pumped back into the feed flow of the membranes. The ERD is used to recover the residual pressure in the discharged brine and transfer it to the feed flow, thereby enhancing the operating efficiency of the SWRO. An auxiliary boost pump is used to control the concentrate flow and offset any pressure losses [15], [11]. For the case of the boost pump connected to the ERD, the amount of flow rate can be adjusted by using power electronics to modify the rotational speed of the pump.

II. Numerical Model Approach

A numerical study of the two direct-driven configurations and control strategies of the integrated tidal turbine with SWRO and ERD is developed to assess the behavior and performance of the system in both steady-state and dynamic conditions. In the following paragraphs, a brief description of the simplified mathematical models of the main components is presented. Similar models have been previously employed by the author in [12]. It is important to highlight the coupling between the physical variables of the modules that have an effect on the system behavior. The set of algebraic and differential equations that describe the fully non-linear coupled model are implemented in MATLAB-Simulink and solved in the time domain based on numerical integration scheme with variable time-step.

A. Tidal turbine rotor

For this evaluation, an existing three bladed horizontal axis turbine with a rotor diameter of 10 m was selected. The hydrodynamic characterization of the rotor is based on the work of [16]–[19]. This rotor delivers high torque values at optimum operating conditions, therefore, deemed suitable for this application. The simplified performance of the rotor is expressed for the hydrodynamic torque and power as a function of the upstream tidal velocity U_c, the water density ρ_w and the rotor radius R, as presented in (1) and (2).

$$\tau_{hydro} = C_\tau(\lambda,\beta)\,\frac{1}{2}\,\rho_w\,\pi\,R^3\,U_c^2 \tag{1}$$

$$P_{aero} = C_P(\lambda,\beta)\,\frac{1}{2}\,\rho_w\,\pi R^2\,U_c^3 \tag{2}$$

The torque and power coefficients C_τ and C_P coefficients are defined as a function of the collective pitch angle of the blades β and the tip speed ratio λ, which is defined as the ratio of the rotor tip tangential speed to the upstream tidal velocity $\lambda = \frac{\omega_r R}{U_c}$. The tangential speed of the rotor is given by the product of the rotor radius and its rotational speed ω_r.

B. Hydraulic desalination system

1) Hydraulic drive train: The horizontal axis tidal rotor is rigidly connected to the rotor shaft which drives the high-pressure pump of the positive displacement type [20]. The change in angular momentum of the rotor pump assembly is determined by the difference between the hydrodynamic torque given by the rotor τ_{hydro}, and the counteracting torque of the water pump τ_p, according to the following equation, where J_r represents the combined mass moment of inertia of the rotor-pump assembly.

$$J_r\dot{\omega}_r = \tau_{hydro}\,(U,\beta,\omega_r) - \tau_p\,(V_p,\omega_r,\Delta p_p) \tag{3}$$

The volumetric flow rate of the seawater pump is determined by the rotational speed of the pump and the so called volumetric displacement V_p, which determines the volume of fluid that is obtained for each rotor revolution. In the case of an active controlled pump, the effective volumetric displacement can be modified. In this work such adjustment is introduced through the factor e_p as shown in (4). The internal leakage losses of the pump are described as a linear function of the pressure difference across the pump Δp through the coefficient C_s [21]. The torque transmitted by the pump is given by the quasi-steady relation given in (5), where mechanical losses are included in the form of viscous torque and a Coulomb friction torque through the coefficients B_p and C_{fp} respectively [21], [22]. The actuator response to modify the variable displacement factor is included as a first order differential equation

according to (6). Here, the reference value $e_{p,ref}$ and a characteristic time constant T_{e_p} are used.

$$Q_p = V_p(e_p)\ \omega_r - C_s\,\Delta p \tag{4}$$

$$\tau_p = V_p(e_p)\ \Delta p + B_p\,\omega_r + C_{fp}\,V_p(e_p)\ \Delta p \tag{5}$$

$$T_{e_p}\frac{d}{dt}e_p = e_{p,ref} - e_p \tag{6}$$

2) Reverse osmosis membranes: For the reverse osmosis desalination process, the solution diffusion model is used to represent the transport mechanism of water across the membranes as well as the retention of salts and ions [23], [24]. The flow rate of each component per unit area that passes across a single membrane is given by the water flux according to the following relation:

$$J_w = K_w(\Delta p - \Delta\bar{\pi}) \tag{7}$$

where K_w represents the water permeability constant, Δp_{RO} is the difference in pressure between the two sides of the membrane and $\Delta\bar{\pi}$ is the osmotic pressure difference. An effective concentration C_{eff} at the feed side of the membrane surface is assumed for the total dissolved solids in order to obtain an average osmotic pressure difference as function of the osmotic pressure coefficient δ and the seawater absolute temperature T [25]. The ratio between the effective and the seawater feed concentration Cf, is given in (9) where the salt rejection R_m represents the ability of the membrane to retain the salts, a is the weighting coefficient and U is the water velocity. The subscripts f, c and p stand for the feed, concentrate and permeate respectively

$$\Delta\bar{\pi} = \delta T C_{eff} \tag{8}$$

$$\frac{C_{eff}}{C_f} = a + (1-a)\left[(1-R_m) + R_m\left(\frac{U_f}{U_c}\right)\right] \tag{9}$$

Considering the mass balance over the RO membrane, the following relation between flow rates is obtained assuming a negligible difference in seawater density:

$$U_f A_f = U_c A_c + U_p A_p \tag{10}$$

An important parameter that characterizes RO membranes is the recovery rate RR, which represents the ratio of membrane permeate or fresh water to the feed water of the system. In practice, the recovery rates of typical SWRO plants are closer to 50% [7],

$$RR = \frac{Q_p}{Q_f} = \frac{U_p A_p}{U_f A_f} \tag{11}$$

3) Isobaric ERD unit: Applying the mass balance principle, a simplified model is derived to obtain the overall mass flow rates of water and solute through the ERD [26].

$$\frac{\mathrm{d}m_{\mathrm{f,out}}}{\mathrm{d}t} = F_{\mathrm{f,in}} + F_{\mathrm{b,in}} - F_{\mathrm{b,out}} \tag{12}$$

$$\text{with}\quad F_{\mathrm{b,out}} = F_{\mathrm{b,in}} + \mathrm{OV}\cdot F_{\mathrm{f,in}} \tag{13}$$

where $m_{f,out}$ refers to the overall mass of the pressurized feed water at the outlet of the ERD unit. The mass flow rates of the influent streams for the feed and brine are described by $F_{f,in}$ and $F_{b,in}$ respectively, whereas $F_{b,out}$ represents the brine effluent. A stream of water is bypassed during each cycle to keep the coordination between all the chambers in the pressure exchanger. This water stream is known as overflush and is determined by the difference between $F_{f,in}$ and $F_{f,out}$, typically expressed as a constant ratio OV with respect to the seawater feed intake [15].

Similarly, the mass balance equation for the solute is expressed as:

$$\frac{\mathrm{d}m_{\mathrm{b,out}}}{\mathrm{d}t} = F_{\mathrm{f,in}}C_{\mathrm{f,in}} + F_{\mathrm{b,in}}C_{\mathrm{b,in}} - F_{\mathrm{f,\,out}}\,C_{\mathrm{f,\,out}} \tag{14}$$

$$\text{with}\quad C_{\mathrm{f,\,out}} = M\,(C_{\mathrm{b,\,in}} - C_{\mathrm{f,\,in}}) + C_{\mathrm{f,\,in}} \tag{15}$$

where $m_{b,out}$ is the solute mass of the depressurized brine, $C_{b,in}$ and $C_{f,in}$ indicate the concentrations of the influent streams for the high pressure brine and low pressure feed, respectively and $C_{f,out}$ represents the concentration of the effluent for the pressurized feed. It is assumed that the increased salinity of the feed stream at the outlet of the ERD and at the entrance of the RO membranes, is given by a constant volumetric mixing ratio M, between the feed and brine streams. This change in salinity is caused by the hydraulic energy transfer in the pressure exchanger.

An auxiliary boost pump is integrated together with the ERD device to compensate for any pressure losses and to regulate the recovery rate of the SWRO. Similarly to the pump actuator model, it is assumed that the boost pump, either with variable speed or variable displacement, has the ability to adjust the recovery rate according to the reference value RR_{ref} and a characteristic time constant T_{ERD} as described by the following differential equation:

$$T_{ERD}\frac{d}{dt}RR = RR_{ref} - RR \tag{16}$$

4) Pitch actuator: The pitch actuator is based on a pitch-servo model described by a proportional regulator with constant K_β [27]. The demanded pitch β_{dem} is obtained from the signal of the pitch controller. The second-order model includes a time constant t_β and an input delay from input u_β to the pitch rate $\dot{\beta}$. During the simulation, the delayed input u_β^δ is implemented by storing the input signal and the simulation time in a buffer for a specified amount of time given by δ. The pitch actuator is implemented with pitch rate limits of $\pm 8\ ^\circ$ per second:

$$\ddot{\beta} = \frac{1}{t_\beta}\left(u_\beta^\delta - \dot{\beta}\right) \tag{17}$$

$$u_\beta = K_\beta\,(\beta_{\mathrm{dem}} - \beta_{\mathrm{meas}}) \tag{18}$$

III. Control Strategies

A. Below rated current speed operation.

For below rated current speeds, the power capture of the turbine rotor is maximized by adjusting its

rotational speed to match the optimal hydrodynamic performance. These conditions occur at a particular tip speed ratio where $C_{P,max}$ is achieved. This control strategy is known as variable speed operation. The well known quadratic relation for the optimal hydrodynamic torque as a function of the rotor speed is obtained by substituting (2) into (1). Using the definition of tip speed ratio, such relation is given by (19)

$$\tau_{hydro,CPmax} = \frac{1}{2}\frac{C_{P,\max}}{\left(\lambda_{C_{P,\max}}\right)^3}\rho_w \pi R^5 \omega_r^2 \tag{19}$$

Conventional tidal turbines use electromechanical transmissions to control the rotor speed by using power electronics to adjust the electromechanical torque provided by the generator. In the absence of electrical machines, as it is the case of hydraulic power transmissions, the rotor speed control is achieved by adjusting the torque transmitted by the high-pressure pump. The pump's torque depends on the system pressure and the volumetric displacement of the pump, both of which can be adjusted separately or simultaneously. The description of two configurations and control strategies for below rated current speed operation of a direct driven tidal stream SWRO system with ERD are described in the following subsections.

1) Constant displacement pump & active controlled ERD: The first configuration uses a high-pressure pump with constant volumetric displacement. Consequently, the pump's torque and therefore the rotor speed are indirectly controlled by adjusting the system pressure through the ERD's boost pump. The idea is to modify the effective concentration and consequently the osmotic pressure induced by the RO membranes by regulating the circulating flow towards them. This configuration only controls the recovery rate of the ERD system depending on the system pressure and rotor speed. The recovery rate of the ERD device is limited to a maximum value of 50%.

2) Variable displacement pump with active control & ERD: The second configuration requires a high-pressure pump with the ability to adjust its volumetric displacement. In this way, the transmitted torque of the pump is directly controlled in a similar way to that of an electromechanical transmission. The volumetric displacement required will depend on the rotor speed and the system pressure. In this configuration, the ERD system is independently controlled to maintain a constant recovery rate. Similar strategies to manipulate the system pressure in hydraulic wind turbines have been presented in [9].

B. Above rated current speed operation.

Above rated current speed, the rated rotor speed is maintained by pitching collectively the rotor blades. A conventional PI pitch controller is proposed using the rotor speed error instead of the generator speed error. Due to the sensitivity of the hydrodynamic response of the rotor to the pitch angle, the value of the controller gains are modified as a function of the pitch angle through a gain-scheduled approach. The gain scheduled PI controller is shown in the next equations, where $K_{\mathrm{P/I}}$ are the proportional and integral gains respectively, $K_{\mathrm{P/I,0}}$ is the gain at rated pitch angle $\beta = 0$, and β_{K} is the blade pitch angle at which the pitch sensitivity of hydrodynamic power to rotor collective blade pitch has doubled from its value at the rated operating point.

$$\beta_{\mathrm{dem}} = K_{\mathrm{P}}(\beta)\omega_{\mathrm{r,\ error}} + K_I(\beta)\int_0^t \omega_{\mathrm{r,\ error}}\,\mathrm{d}t \tag{20}$$

$$K_{\mathrm{P/I}}(\beta) = K_{\mathrm{P/I,0}}\frac{\beta_{\mathrm{K}}}{\beta_{\mathrm{K}}+\beta} \tag{21}$$

$$\omega_{\mathrm{r\ ,\ error}} = \omega_{\mathrm{r,\ rated}} - \omega_{\mathrm{r,\ meas}} \tag{22}$$

The values of the different gains are obtained in a similar way as with wind turbines taking into account a modified apparent inertia at the low-speed shaft and a transmission ratio set to one [11]. This approach was originally proposed in [28] and was adapted in this work to hydrokinetic turbines.

IV. Case study

The performance of the configurations and control strategies described in the previous section is compared using a 10 m rotor diameter tidal turbine. The turbine has a rated current speed of 2.0 m/s and rated power of 140 kW. An intake feed concentration of 35500 ppm was used for the seawater feed conditions. The operating range of the integrated turbine and SWRO system is given by the equilibrium points between the rotor torque-speed characteristics and the torque-speed load induced by the high pressure pump driving the SWRO unit. The resulting torque and power curves are shown for different rotor speeds in Fig. 2a and Fig. 2b. The graphical results provide insight into the variable speed operation together with the system torque and power.

The resulting operating conditions for the two studied configurations are summarized in Table I.

TABLE I
MAIN OPERATIONAL PARAMETERS

	Fixed disp. pump with active control ERD	Active control pump with ERD
Rated current speed (m/s)	2.0	2.0
Rated power (kW)	129	139
Rated torque (kNm)	58.2	93.7
Rated rotor speed (rpm)	21.1	14.2
Rated power coefficient C_P	0.38	0.42
Permeate flow rate (m3/h)	80.5	88.3
Rated system pressure (bar)	54.2	55.2
Minimum system pressure (bar)	31.2	44.3

For the case of a constant displacement pump, it is shown that for low rotor-speeds a minimum torque is required to overcome the osmotic pressure which is only achieved after 1.0 m/s. Between current speeds of 1.0 and 1.5 m/s, the recovery rate of the ERD unit is able to adjust the system pressure in such a way that the rotor can follow the ideal rotor speed-torque

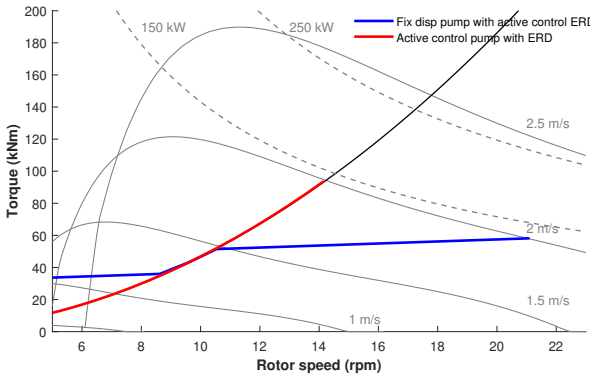

(a) Torque and rotor speed.

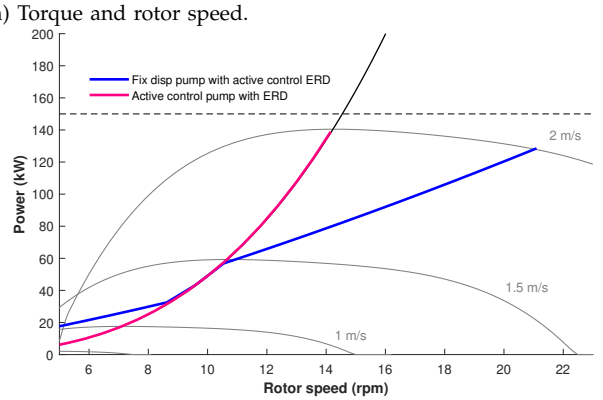

(b) Mechanical power and rotor speed.

Fig. 2. Torque and power speed curve used to define the variable speed control for below rated current velocities.

quadratic relation defined by the optimal tip speed ratio i.e. where maximum power coefficient occurs. However, after 1.5 m/s the maximum recovery rate of 50% is reached, consequently lower concentrations are observed, resulting in lower osmotic pressures induced by the membranes. Without the capacity of increasing the pressure above certain level, the ideal torque can only be achieved for a limited range of current speeds. Once the maximum recovery rate is reached, the rotor follows a linear relation with respect to the torque. The lower torques result in a higher range of operational rotor speeds, which can reach up to 21.1 rpm for a rated speed of 2 m/s.

For the case of the active control pump with ERD, it is possible to follow the variable speed relation for optimal hydrodynamic performance throughout the full operating range, while maintaining a constant recovery rate of 50%. With this configuration and control strategy, a maximum rotor speed of 14.2 rpm is reached at rated current speed of 2 m/s. A different way to ilustrate the harnessed power and torque for the entire range of operational current speeds is shown in Fig. 3. The main parameters of the tidal and SWRO numerical model are shown in Table II.

V. Results

A. Steady-state operating points

The first set of results shows the operational window of the integrated system under steady-state conditions for a range of current speeds. The comparison is shown for the two configurations discussed under steady-state conditions.

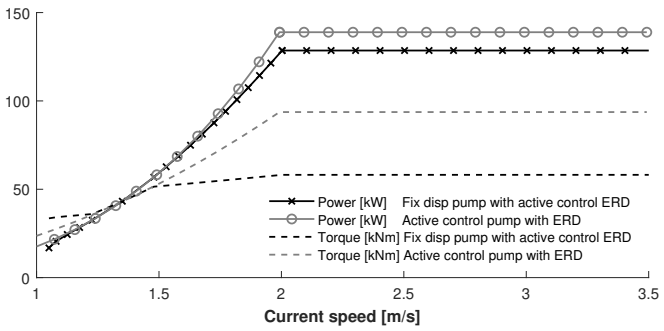

Fig. 3. Steady-state mechanical power and torque for tidal stream SWRO system with ERD.

TABLE II
Numerical Model Parameters

Symbol	Quantity	Unit	Value
ρ_w	Seawater density	kg/m^3	1025
Cf_{in}	Intake feed concentration	ppm	35500
R	Rotor radius	m	5
J_r	Rotor-pump inertia	kg·m^2	1.0e5
V_p	Pump volumetric size	L/rev	66.13
C_s	Pump's leakage coeff	m^3/(sPa)	1.5e-10
B_p	Pump's viscous coeff	Nm·s	0.0
C_{fp}	Pump's friction coeff	-	0.02
K_w	Mass transfer coeff[a]	s/m	6.4e-9
N_m	Number of membranes	-	404
A_m	Area per membrane[a]	m^2	7.34
A_f	Feed flow pipe area	m^2	9.1e-3
A_c	Concentrate pipe area	m^2	9.1e-3
A_p	Permeate pipe area	m^2	5.5e-3
δ	Osmotic pressure coeff	Pa/(ppm K)	0.2641
R_m	Fractional salt rejection[a]	-	0.97
a	Concentration weight coeff	-	0.5
OV	Overflush ratio of ERD	-	0.05
M	Volumetric mixing of ERD	-	0.06
T_{ERD}	ERD time constant	s	4.0
T_{e_p}	Pump actuator time constant	s	2.0

[a] The water permeability was estimated empirically from commercial RO membranes data corresponding to the DOW FILMTEC^{TM} SW30-4040, a thin film composite membrane consisting of three layers: a polyester support web, a microporous polysulfone interlayer and an ultra-thin polyamide barrier layer on the top surface.

The first plot in Fig. 4a shows that the configuration with variable displacement pump has a linear relation, i.e. a constant tip speed ratio is achieved for below rated conditions. In contrast, the fixed pump configuration with controlled ERD shows lower rotational speeds between 1 and 1.5 -m/s, and much higher rotational speeds between 1.5 and 2.0 m/s, displaying also a linear relationship but with a greater slope.

In Fig. 4b it is observed that the system pressure for the variable displacement pump configuration also has a linear relationship with values between 42 and 55 bar at rated current speed. A constant osmotic pressure of 42 bar is shown throughout the operating current speeds. The fixed pump configuration with controlled ERD shows a wider pressure range between

31 and 54 bar with osmotic pressures values between 28 and 42 bar. The permeate flow rate or fresh water production is also shown in Fig. 4c.

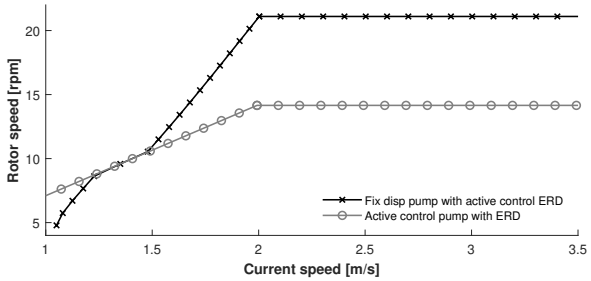

(a) Rotor-pump speed for operating current velocities.

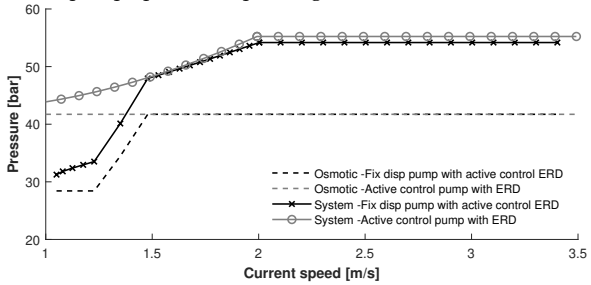

(b) Pressure for operating current velocities.

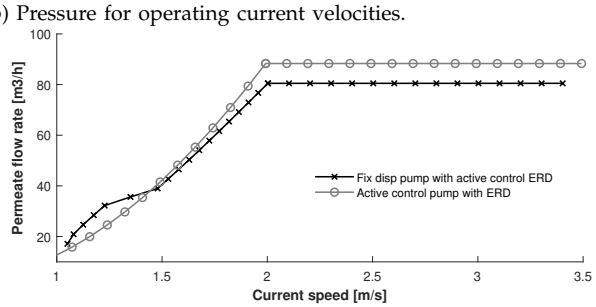

(c) Fresh water production for operating current velocities.

Fig. 4. Steady-state rotor speed, pressure and permeate production for tidal stream SWRO system with ERD.

The specific energy consumption (SEC) was obtained for the two configurations. In the operating range of current speeds, the SEC was between 2.8 to 15 kWh/m3, and 2.6 to 4.2 kWh/m3, for the fixed displacement pump and the active control pump respectively. At rated speed conditions, both configurations show an average SEC of 3.2 kWh/m3. These values are very much aligned with the experimental results in [5], where the system's SEC is reported at 3.61 kWh/m3, with an energy recovery efficiency of 83.7%. Moreover, the values obtained above are within range of SECs reported in SWRO plants [29] without including pre-treatment and post-treatment processes.

B. Response to stochastic current velocity

The second set of results allow to compare the dynamic response of the coupled integrated tidal stream SWRO system, through time-domain simulations under a given stochastic current speed. The simulations were performed using an artificial time series for 800 s for an average current speed of 1.6 m/s and turbulence intensity of 14% as shown in Fig. 5. See the appendix for further details on the model to generate the time series. The first 200 s of the simulations were accounted for transient effects. The results of the comparison between the time series of the rotor speed, the system pressure, the permeate flow rate, and recovery rate are shown in separate graphs in Fig. 6.

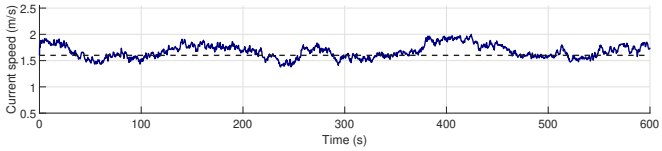

Fig. 5. Current speed time series with 1.6 m/s mean value and 14% turbulence intensity used for the time-domain simulations.

It is observed that for the fixed displacement pump configuration, the rotor speed experiences higher excursions and lower pressures compared to the active controlled pump. It is observed that a pressure difference between the two configurations of around 1 bar is maintained for most part of the simulation. However, significant pressure drops of up to 6 bars occur for the fixed pump configuration when current speeds drops below 1.5 m/s. For the active controlled pump, the system pressure is kept between a range of 46.9 and 54.5 bars, well within the operating range of the SWRO system. Higher fresh water production is achieved with the active controlled pump as the recovery rate is kept at a relatively constant value of 50%.

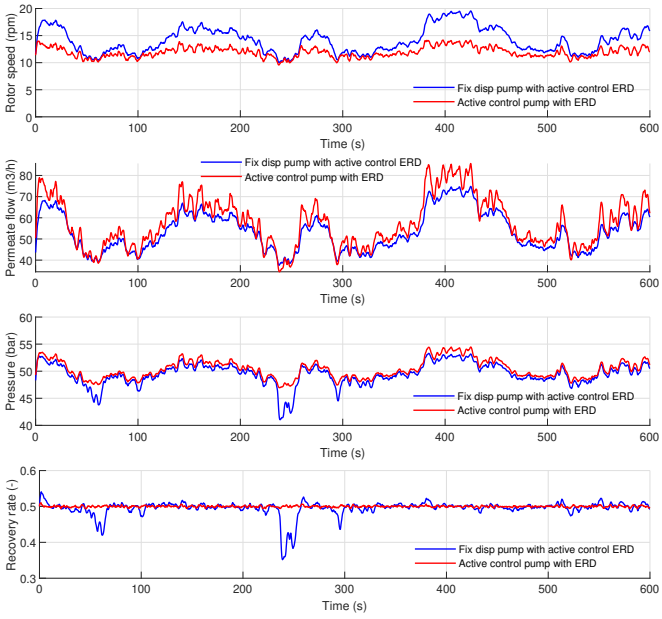

Fig. 6. Time-domain results for the rotor and the SWRO system response subject to turbulent current speed conditions with 14.0% TI.

The comparison of the simulation results for the two configurations is summarized in Fig. 7 for the production of fresh water under turbulent conditions. Despite lower fluctuations in rotational speed and pressure, the active controlled pump configuration shows a clear increase in permeate flow rate. In addition, the higher fluctuations in the permeate flow rate are shown around the average value of 56 m^3/h. When the turbine operated at the turbulence intensity level of 14%, an increase of 8% of fresh water production

was obtained compared to the average cumulative permeate output.

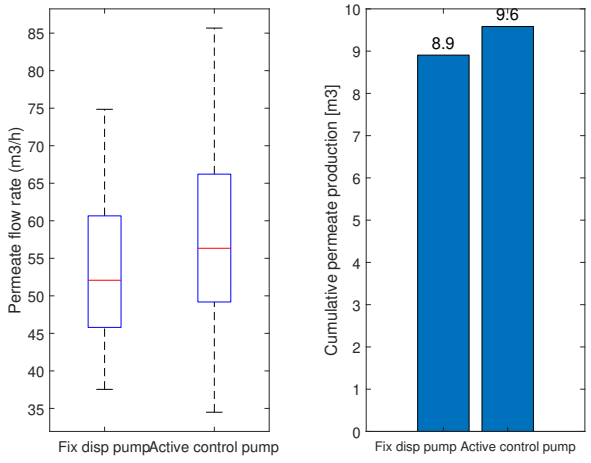

Fig. 7. Comparison of simulation results for fresh water flow rate and production. The average current speed is $\bar{U} = 1.6$ m/s, with 14.0% turbulence intensity and simulations of 600 s.

While the fixed displacement pump is in general a much simpler configuration. The higher rotational speeds of the rotor might lead to potential problems regarding cavitation and fatigue, without mentioning the additional limitations of having a controlled ERD. In contrast, a high-pressure, variable displacement pump for seawater is a more complex component. Further consideration should be taken to consider both limitations in the system design.

VI. Conclusions

This study evaluated the performance of a direct-driven tidal stream reverse osmosis desalination system under both steady-state and dynamic flow conditions, comparing two configurations: one employing a fixed displacement pump with an actively controlled energy recovery device, and another using a variable displacement pump. The steady-state results demonstrated that the variable displacement pump maintained a constant tip speed ratio below rated current velocities, yielding to a more stable operating behavior. In contrast, the fixed pump configuration exhibited a wider operating range in both rotational speed and system pressure. The specific energy consumption across both configurations fell within typical ranges for SWRO systems, with the actively controlled configuration achieving lower SEC values in the range of 2.6 to 4.2 kWh/m3. At rated current speed conditions, freshwater production is up to 88.3 m3/h with a SEC of 3.2 kWh/m3. Under stochastic current conditions, the time-domain simulations highlighted that the active control strategy led to improved operational stability and higher freshwater production. Specifically, for an average current speed of 1.6 m/s with 14% turbulence intensity, a cumulative increase of 8% in permeate flow was observed for the controlled pump configuration, while also maintaining a relatively constant recovery rate around 50%. These results suggest that adopting an actively controlled hydraulic transmission system in direct-driven tidal desalination turbines can enhance system performance, stabilize operation under fluctuating tidal currents, and ultimately increase freshwater output. This work highlights the potential and challenges of integrating tidal energy directly into desalination processes and provides insights into system optimization under realistic operating conditions. Future work will aim to refine the control strategies and explore the long-term reliability and scalability of such integrated systems.

Appendix
Time Series of the Tidal Resource

A series of artificial time series of the rotor-average current speeds are simulated for a defined turbulence intensity level. The turbulence velocity fluctuations u' were generated at hub height according to the model spectra for the three tidal components, K, as a function of the component-turbulent kinetic energy (TKE) levels σ_K^2 and the vertical velocity shear $\partial u/\partial z$ as proposed by [30]:

$$S_K(f) = \frac{\sigma_K^2 s_{1,K} \left(\frac{\partial u}{\partial z}\right)^{-1}}{1 + s_{2,K}\left(\frac{f}{\partial u/\partial z}\right)^{5/3}} \tag{23}$$

where f is the cyclic frequency and the two scales, s_1 and s_2, are empirically defined for each component as follows:

$$\langle s_{1,K}, s_{2,K}\rangle = \begin{cases} \langle 1.21, 4.30\rangle & K = u \\ \langle 0.33, 0.50\rangle & K = v \\ \langle 0.23, 0.26\rangle & K = w \end{cases} \tag{24}$$

The component-TKE levels are determined based on an exponential profile proportional to the the friction velocity input parameter U^*:

$$\sigma_K^2 = {U^*}^2 \mu_K e^{-2d/H_{ref}} \tag{25}$$

where d is the water depth, H_{ref} is the reference hub height above seabed and $\mu_u = 4.5$, $\mu_v = 2.25$ and $\mu_w = 0.9$, are empirically determined coefficients whose values are obtained from [31].

References

[1] M. A. Abdelkareem, M. E. H. Assad, E. T. Sayed, and B. Soudan, "Recent progress in the use of renewable energy sources to power water desalination plants," *Desalination*, vol. 435, pp. 97–113, 2018.

[2] I. Nurjanah, T.-T. Chang, S.-J. You, C.-Y. Huang, and W.-Y. Sean, "Reverse osmosis integrated with renewable energy as sustainable technology: A review," *Desalination*, vol. 581, p. 117590, 2024.

[3] J. Leijon, J. Forslund, K. Thomas, and C. Boström, "Marine current energy converters to power a reverse osmosis desalination plant," *Energies*, vol. 11, no. 11, p. 2880, 2018.

[4] E. Dimitriou, J. Camacho-Espino, A. Anastasiou, and G. Papadakis, "Experimental investigation of the performance of a seawater reverse osmosis desalination system operating under variable feed flowrate pressure and temperature conditions," *Journal of Environmental Chemical Engineering*, vol. 13, no. 2, p. 115778, 2025.

[5] Y. Gu, T. Zou, H. Ren, H. Liu, Y. Lin, Z. Song, and K. Ye, "The reverse osmosis desalination system driven by the marine current turbine under dynamic conditions," *Desalination*, vol. 614, p. 119142, 2025.

[6] K. A. Sitterley, T. J. Cath, D. S. Jenne, Y.-H. Yu, and T. Y. Cath, "Performance of reverse osmosis membrane with large feed pressure fluctuations from a wave-driven desalination system," *Desalination*, vol. 527, p. 115546, 2022.
[7] T. K. Das, M. Folley, P. Lamont-Kane, and C. Frost, "Performance of a swro membrane under variable flow conditions arising from wave powered desalination," *Desalination*, vol. 571, p. 117069, 2024.
[8] T. K. Das, C. Frost, M. Folley, and P. Brewster, "Application of an energy recovery device with ro membrane for wave powered desalination," *Desalination*, vol. 592, p. 118064, 2024.
[9] F. Greco, D. De Bruycker, A. Velez-Isaza, N. Diepeveen, and A. Jarquin-Laguna, "Preliminary design of a hydraulic wind turbine drive train for integrated electricity production and seawater desalination," in *Journal of Physics: Conference Series*, vol. 1618, no. 3. IOP Publishing, 2020, p. 032015.
[10] F. Greco, S. G. Heijman, and A. Jarquin-Laguna, "Integration of wind energy and desalination systems: a review study," *Processes*, vol. 9, no. 12, p. 2181, 2021.
[11] A. Jarquin-Laguna and F. Greco, "Integration of hydraulic wind turbines for seawater reverse osmosis desalination," in *2019 Offshore Energy and Storage Summit (OSES)*, July 2019, pp. 1–9.
[12] A. Jarquin-Laguna and S. Ordonez-Sanchez, "Utilising tidal stream energy to drive seawater reverse osmosis desalination processes," in *Proceedings of the European Wave and Tidal Energy Conference*. European Wave and Tidal Energy Conference, 2021, p. 2143.
[13] C. Fritzmann, J. Löwenberg, T. Wintgens, and T. Melin, "State-of-the-art of reverse osmosis desalination," *Desalination*, vol. 216, no. 1-3, pp. 1–76, 2007.
[14] A. Jarquin-Laguna and F. Greco, "Effects of recovery rate on variable speed direct-driven tidal energy desalination," in *Paper presented at PAMEC 2024*, ser. Pan American Marine Energy Conference, Barranquilla, Colombia, feb 2024. [Online]. Available: https://pamec.energy/events/pamec2024/conference-program/
[15] R. L. Stover, "Seawater reverse osmosis with isobaric energy recovery devices," *Desalination*, vol. 203, no. 1-3, pp. 168–175, 2007.
[16] S. Ordonez-Sanchez, M. Allmark, K. Porter, R. Ellis, C. Lloyd, I. Santic, T. O'Doherty, and C. Johnstone, "Analysis of a horizontal-axis tidal turbine performance in the presence of regular and irregular waves using two control strategies," *Energies*, vol. 12, p. 367, 2019, impact factor: 2.7.
[17] R. Martinez, S. Ordonez-sanchez, C. M. Johnstone, M. Allmark, C. Lloyd, T. O'Doherty, B. Gaurier, and G. Germain, "Analysis of the effects of control strategies and wave climates on the loading and performance of a laboratory scale horizontal axis tidal turbine," *In Review*, 2019.
[18] M. Allmark, R. Ellis, C. Lloyd, S. Ordonez-Sanchez, K. Johannesen, C. Byrne, C. Johnstone, T. O'Doherty, and A. Mason-Jones, "The development, design and characterisation of a scale model horizontal axis tidal turbine for dynamic load quantification," *Renewable Energy*, vol. 156, pp. 913–930, 2020. [Online]. Available: https://www.sciencedirect.com/science/article/pii/S0960148120305929
[19] M. Allmark, R. Ellis, T. Ebdon, C. Lloyd, S. Ordonez-Sanchez, R. Martinez, A. Mason-Jones, C. Johnstone, and T. O'Doherty, "A detailed study of tidal turbine power production and dynamic loading under grid generated turbulence and turbine wake operation," *Renewable Energy*, vol. 169, pp. 1422–1439, 2021. [Online]. Available: https://www.sciencedirect.com/science/article/pii/S0960148120319789
[20] W. Chen, X. Wang, F. Zhang, H. Liu, and Y. Lin, "Review of the application of hydraulic technology in wind turbine," *Wind Energy*, vol. 23, no. 7, pp. 1495–1522, 2020.
[21] H.-S. Jeong and H.-E. Kim, "A novel performance model given by the physical dimensions of hydraulic axial piston motors: Experimental analysis," *Journal of mechanical science and technology*, vol. 21, no. 4, pp. 630–641, 2007.
[22] H. E. Merritt and V. Pomper, "Hydraulic control systems," *Journal of Applied Mechanics*, vol. 35, no. 1, p. 200, 1968.
[23] M. Qasim, M. Badrelzaman, N. N. Darwish, N. A. Darwish, and N. Hilal, "Reverse osmosis desalination: A state-of-the-art review," *Desalination*, vol. 459, pp. 59–104, 2019.
[24] J. G. Wijmans and R. W. Baker, "The solution-diffusion model: a review," *Journal of membrane science*, vol. 107, no. 1-2, pp. 1–21, 1995.
[25] A. R. Bartman, P. D. Christofides, and Y. Cohen, "Nonlinear model-based control of an experimental reverse-osmosis water desalination system," *Industrial & Engineering Chemistry Research*, vol. 48, no. 13, pp. 6126–6136, 2009.
[26] K. Jeong, Y. G. Lee, S. J. Ki, and J. H. Kim, "Modeling seawater reverse osmosis system under degradation conditions of membrane performance: assessment of isobaric energy recovery devices and feed pressure control benefits," *Desalination and Water Treatment*, vol. 57, no. 43, pp. 20 210–20 218, 2016.
[27] A. Jarquin Laguna, "Simulation of an offshore wind farm using fluid power for centralized electricity generation," *Wind Energy Science*, vol. 2, no. 2, pp. 387–402, 2017.
[28] J. Jonkman, S. Butterfield, W. Musial, and G. Scott, "Definition of a 5-mw reference wind turbine for offshore system development," National Renewable Energy Lab.(NREL), Golden, CO (United States), Tech. Rep., 2009.
[29] J. Kim, K. Park, D. R. Yang, and S. Hong, "A comprehensive review of energy consumption of seawater reverse osmosis desalination plants," *Applied Energy*, vol. 254, p. 113652, 2019.
[30] B. J. Jonkman, M. L. Buhl, and N. R. E. L. (U.S.), *TurbSim user's guide [electronic resource] / B.J. Jonkman and M.L. Buhl, Jr.* National Renewable Energy Laboratory Golden, Colo, 2006.
[31] J. Thomson, B. Polagye, V. Durgesh, and M. C. Richmond, "Measurements of turbulence at two tidal energy sites in puget sound, wa," *IEEE Journal of Oceanic Engineering*, vol. 37, no. 3, pp. 363–374, 2012.